Polymer 138 (2018) 203–210

Contents lists available at ScienceDirect

Polymer

journal homepage: www.elsevier.com/locate/polymer

Polydimethylsiloxane-titania nanocomposite coating: Fabrication and corrosion resistance

Xiaokun Cui [a], Guiyu Zhu [a], Yufeng Pan [a], Qian Shao [b], Cindy (xinxin) Zhao [c], Mengyao Dong [c, d], Yue Zhang [a, *], Zhanhu Guo [c, **]

[a] Institute of Material Science and Engineering, Ocean University of China, Qingdao, Shandong, 266100 PR China
[b] College of Chemical and Environmental Engineering, Shandong University of Science and Technology, Qingdao 266590, PR China
[c] Integrated Composites Laboratory (ICL), Department of Chemical Engineering, University of Tennessee, Knoxville, TN 37996, USA
[d] National Engineering Research Center for Advanced Polymer Processing Technology, Zhengzhou University, Zhengzhou 450002, PR China

ARTICLE INFO

Article history:
Received 9 December 2017
Received in revised form
11 January 2018
Accepted 22 January 2018
Available online 3 February 2018

Keywords:
PDMS/TiO_2
Corrosion resistance
Composite coatings

ABSTRACT

Titania (TiO_2) nanoparticles were added to polydimethylsiloxane (PDMS) matrix to form nanocomposite coating via spin coating method on the AA 2024 (one of the aluminum alloys) to improve the anticorrosion ability of metal. The microstructures of the PDMS/TiO_2 composite coating were detected by scanning electron microscopy (SEM) and Fourier transform infrared (FTIR) spectrometry to verify the structure of composite coating. The corrosion properties of PDMS/TiO_2 composite coating was evaluated by the electrochemical tests. The results showed that the anticorrosion ability of the composite coating has been significantly affected by the TiO_2 content. For example, the impedance modulus value reached 10^6 Ωcm^2 of the composite coating with 8 wt % nano-TiO_2 fillers. Meanwhile, the corrosion current density (I_{corr}) of the coating was smaller than that of bare aluminum. The long term immersion experiments of coating were performed and the results demonstrated that the coating still had a protective effect on aluminum after 40 days of immersion.

1. Introduction

With a great combination of easy processing, high durability and wide range of applications [1], AA2024 (one of the aluminum alloys) has been widely used in architecture, aviation, etc. Although aluminum alloy has some advantages in many applications, there are still many environmental factors that can cause its corrosion [2,3]. As we all know, the corrosion of materials brings about a lot of problems to our life and it causes a lot of damages to the economy, health and safety. Generally, there are various methods to protect metals from corrosion [2]. For example, the control and protection of metals from corrosion can be achieved by using various coatings [4–11]. The conventional methods of metal protection are usually coating with chromium (VI) based compounds. However, Cr^{6+} ions are toxic and could cause a lot of damages to our health and environment. Therefore, the search for environmentally friendly method for metal protection is very urgent [1,12,13].

Organic coatings are the best choice for corrosion protection because of low cost and versatility. For example, Abaci et al. prepared polyaniline (PANI) and TiO_2 nanoparticles composite coating to protect stainless steel [14]. Hikku et al. constructed graphene/polyvinyl alcohol coatings for protecting metal from corrosion [15]. Organic coatings provide an isolating protective barrier between corrosive environment and metal surface [16–20]. Particularly, hydrophobic and superhydrophobic coatings delay the rate of penetration of water and ions into the substrate [21–26]. Organic coatings could reduce corrosion for two reasons. On one hand, the barrier cannot prevent diffusion of corrosive ion but it can delay the diffusion of oxygen and water and prohibit the formation of fast channel for corrosive ions to protect metal [27]. On the other hand, the organic coatings have good compactness and obstruct the flow of the current.

The main chain of PDMS is made up of-Si-O-Si- structure and side chains of the $-CH_3$ groups. The -Si-O-Si-structure has a high bond energy and large bond angle which give good thermal stability and elasticity of PDMS. The $-CH_3$ groups are hydrophobic and non-polar groups, which make PDMS have a low surface energy and good hydrophobicity. PDMS has been applied in many fields

* Corresponding author.
** Corresponding author.
E-mail addresses: zhangyue@ouc.edu.cn (Y. Zhang), zguo10@utk.edu (Z. Guo).

https://doi.org/10.1016/j.polymer.2018.01.063
0032-3861/

because of the structural characteristics of PDMS. For example, Wang et al. prepared carbon nanotubes/PDMS nanocomposites by a self-segregated structure to enhance electrical conductivity [28]. Sun et al. prepared flexible conductive metacomposites by using MWCNTS and PDMS [29]. Wu et al. investigated the effect of length of different PDMS chains on corrosion resistance [30]. Li et al. prepared superhydrophobic PDMS/SiO_2 composite coatings by spraying. The results show that the contact angle (CA) of the coating is 153° [31]. Kim et al. reported ultra-thin oxide protective coatings on the copper particles by using thermal evaporation of PDMS [32]. Yeo et al. constructed hydrophobic surface of PDMS [33]. Zhao prepared PDMS hybrid thin films using sol-gel method [34]. Yuan et al. fabricated superhydrophobic PDMS/$CaCO_3$ composite coating with a CA of 160° and a sliding angle of 3° [35].

However, some existing microspores and microcracks in the organic coatings lead to poor durability of corrosion resistance. Nanoparticles are found to have apparently improved the corrosion resistance of organic coatings. The nanoparticles including SiO_2 [36], Al_2O_3 [37], ZnO [38] and TiO_2 [39] have demonstrated better protection than micron size particles owing to their higher specific surface area and smaller particle size [40]. For instance, Ejenstam et al. reported superhydrophobic PDMS-20 wt % SiO_2 composite coating with high impedance modulus value of $> 10^9\,\Omega\,cm^2$ at 0.01 Hz and a stable long term corrosion protection in NaCl solution about 90 days [41]. TiO_2 has photocatalytic activity and can kill the bacteria on the metal substrate, making substrate have an anti-fouling and self-cleaning effect [42–45]. Meanwhile, TiO_2 produces a large number of electrons under ultraviolet light and has the effect of photocathode protection, thereby, inhibiting the corrosion of metals. For example, Qing et al. [46] reported the best superhydrophobic TiO_2 coating with a CA of 162.3° and a sliding angle of 4.3° when the content of PDMS was 30 wt%. The I_{corr} of coating with 2.3×10^{-6} A/cm^2 was relatively large to protect copper. Meanwhile, the influence of UV irradiation on the corrosion resistance and CA was also studied, the results presented that the corrosion potential (E_{corr}) shifted negatively and the I_{corr} increased and the contact angle was changed from superhydrophobic to hydrophilic compared with the situation without UV irradiation. However, the effect of the TiO_2 content on the protective effect of metal has not been investigated. Immersion tests were not performed to show durability of the nanocomposite coatings.

In this research, PDMS/TiO_2 composite coatings containing different content of TiO_2 nanoparticles were prepared. The chemical structure of the coating and the surface morphology of the coating were examined by FTIR and SEM respectively. The corrosion resistance of coatings is evaluated by Tafel polarization (Tafel) and impedance (EIS) and the long-term protective properties of the coatings are also discussed.

2. Experiment

2.1. Materials

The AA 2024 substrate was cut into slices of a certain size. Next, the AA2024 samples were grounded with Sic papers (400/800/1200/2000 grit sizes), Then, polishing by diamond paste. Next, they were washed with acetone, ethanol, and water for certain minutes in turn. Finally, they were washed with two percent of NaOH solution for 5 s and dried with nitrogen. The hydroxyl-terminated polydimethylsiloxane (HO-PDMS-OH) (molecular weight of about 2500) was provided from Jinan Xingfeilong Chemical Company. Tetraethoxysilane (TEOS) and dibutyltin dilaurate (DBTDL) were acquired from Sinopharm Chemical Reagent Co. Ltd. Nano-TiO_2 (diameter of 5–10 nm) was purchased from Aladdin Company.

2.2. Preparation of PDMS/TiO_2 coating

The PDMS/TiO_2 coating was prepared as follows. Mixtures of 5 g PDMS and different contents of TiO_2 (4, 6, 8, and 10 wt %) nanoparticles were stirred for 12 h using an impeller set to approximately 1000 rpm. Then, 0.5 g curing agent of TEOS and 0.05 g catalyst of DBTDL were mixed in the above mixture by vigorous magnetic stirring for 6 h. Finally, the solution was applied to the bare AA 2024, and the PDMS/TiO_2 coating was obtained after curing at 120 °C for 2 h. Fig. 1 shows the schematic illustration of preparing PDMS/TiO_2 coating.

2.3. Characterization

FT-IR (Nicolet iN10) within a range of 4000–500 cm^{-1} was used to characterize the chemical composition of the structure. The SEM (HitachiS-4800) was used to observe the micro morphology of the coating. The electrochemical performance tests were performed using CHI606 and the anticorrosion properties of samples were characterized by Tafel and EIS in 3.5 wt% NaCl solution.

3. Results and discussions

3.1. FTIR spectra of samples

Fig. 2 depicts the FT-IR spectra of initial PDMS and TEOS-PDMS and TiO_2/TEOS-PDMS. The stretching vibration of O-H leads to the peaks at 3288 cm^{-1}, the peaks at 2954 and 1088 cm^{-1} are from the stretching vibrations of CH_3 and Si–O–Si groups [47]. The peak near 1250 cm^{-1} is the symmetric deformation of the CH_3 group, the peaks at 887 and 796 cm^{-1} can be the stretching vibrations of Si–C and Si–O [48]. Compared to the spectra of the PDMS, the peaks at 3288 cm^{-1} disappear in the spectra of TEOS-PDMS, indicating that

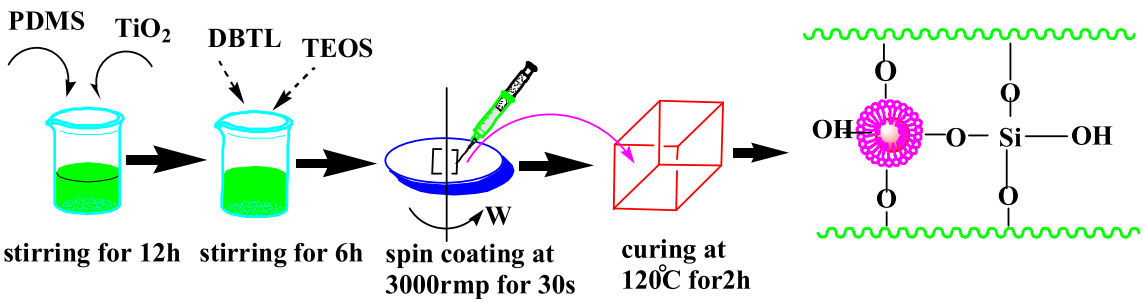

Fig. 1. Schematic illustration for the preparation of PDMS/TiO_2 coating.

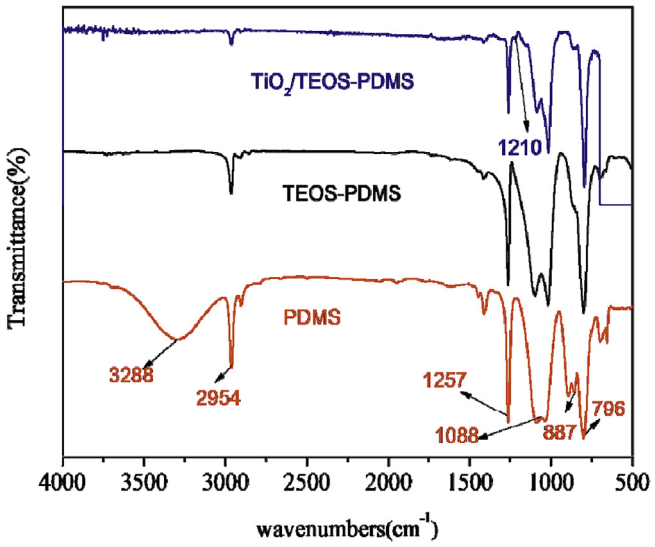

Fig. 2. FTIR spectra of TEOS-PDMS and PDMS and TiO_2/TEOS-PDMS.

the PDMS has reacted with the TEOS. The peak at 1210 cm^{-1} is the stretching vibrations of Si—O—Ti [49]. The presence of feature peaks indicates that TiO_2 and PDMS or TEOS are chemically bonded together. Fig. 3 shows three different reactions, such as the reaction of TiO_2 and PDMS, the reaction of TiO_2 with TEOS and the reaction of PDMS with TEOS. As shown in the graphical abstract, blue clusters represent a large number of hydroxyl groups on the surface of TiO_2. Through the above reaction, TiO_2 was tightly loaded on the PDMS coating.

3.2. Microstructure

Fig. 4 shows the SEM images of the composites with different

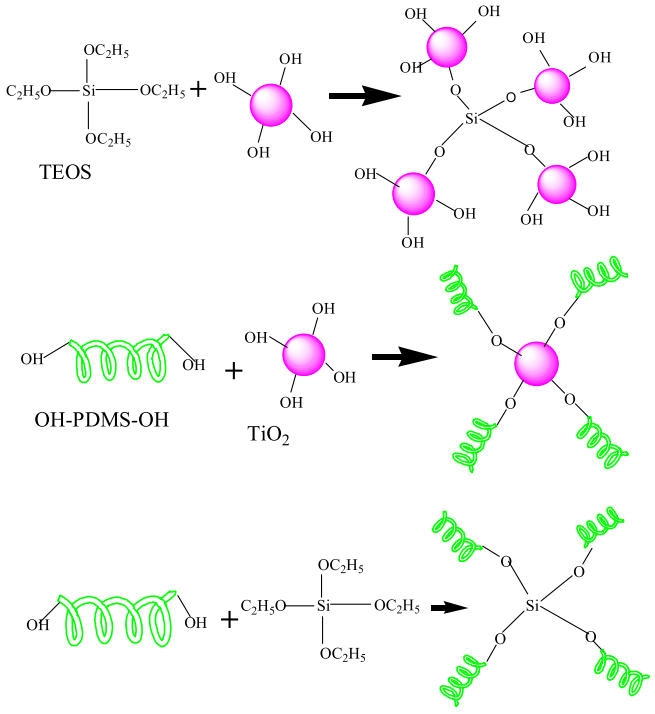

Fig. 3. Schematic illustration for the reaction of TiO_2, PDMS and TEOS.

TiO_2 loading levels. Micron-sized particles were observed arising from the agglomeration of the nano-TiO_2 with large surface energy and strong interaction, shaping hierarchical micro/nano rough structures on the surface. When the content of TiO_2 was 4 wt % in Fig. 4 (a), the diameter of the smaller agglomerated particles was 5 μm and the larger one was 12.5 μm. When the content of TiO_2 was 6% in Fig. 4 (b), the smaller diameter was 6.7 μm and the larger was 15.3 μm. When the content of TiO_2 was less than 8 wt%, the dispersion of TiO_2 in PDMS coating was relatively uniform. However, the amount of TiO_2 in the surface of the coating was less than 8 wt %; the formation of micro-nano structure was less. When the TiO_2 content was 8 wt % in Fig. 4(c), the diameter of the smaller was 7.5 μm and the larger one was 15.5 μm. TiO_2 covered most areas of the coating and formed more micro-nano structures. When the content of TiO_2 was relatively high, namely 10 wt % in Fig. 4 (d), the dispersion of TiO_2 was relatively poor and destroyed the uniformity of coating structure.

3.3. Hydrophobic properties of coatings

In general, when the contact angle of the material was greater than 90°, it can be called a hydrophobic material. The hydrophobic materials had two characteristics. One was low surface energy, and the other was rough structure. Because PDMS contained a large number of hydrophobic groups, it had a low surface energy and a certain self-cleaning effect. The CA of PDMS coating was about 102° (Fig. 5). When hydrophilic TiO_2 was added to the PDMS, the coatings with micro-nano rough structure have a larger amount of air which blocks the entry of water, which influence the CA of surface (see Fig. 5). On one hand, the hydrophilic properties of TiO_2 coating would decrease the CA. When the content of TiO_2 was low (4 and 6 wt %), the CA of coating was decreased from 102° to 98°. Because the content of TiO_2 on the surface of the coating is less, the number of micro-nano structures is less (Fig.4 (a) and (b)). On the other hand, the addition of TiO_2 would increase the roughness of the composite coating, thereby increasing the CA. When the content of TiO_2 was high (8 and 10 wt %), the formed more micro-nano structures changed the CA of coating (Fig.4 (c) and (d)). The rough structure of coating surface played a major role and the CA of coating was increased from 98° to 108°. If the content of TiO_2 was too high, the uniformity of TiO_2 in the coating was destroyed, causing a decreased CA of composite coatings [28].

3.4. Corrosion resistance of coatings

3.4.1. Impedance results

Fig. 6 depicts the impedance graph of different sample in 3.5 wt % NaCl solution. Compared with AA-2024, the impedance modulus value of coating is greatly improved. Obviously, two capacitive semicircles are observed in Fig. 6 (a) (The illustration is the equivalent circuit). Fig. 6 (a1) is local enlarged drawing of Fig. 6 (a). In regions with relatively high frequency, the capacitive arc might be interpreted as the coating capacitance (CPE_{coat}) and the coating resistance (R_f) [50]. In areas with low frequency, the capacitive arc could be put down to the double layer capacitance (CPE_{dl}) and the charge transfer resistance (R_{ct}) [51]. Fig. 6 (b) depicts the Bode graph of sample with different amounts of TiO_2 (4, 6, 8, and 10 wt %) to verify the effect of TiO_2 content on the anticorrosion performance. As depicted in Fig. 6 (b), the impedance modulus value of bare aluminum at lower frequencies is only $10^4\,\Omega\,cm^2$ and the impedance modulus value of the PDMS coating without TiO_2 is $10^5\,\Omega\,cm^2$ in areas with low frequency. With the increase of TiO_2 content, micro-nano structure appear on the surface of sample (Fig. 4). Thus, it was difficult for the corrosion ions to pass through the coating and touch the substrate, improving the anticorrosion

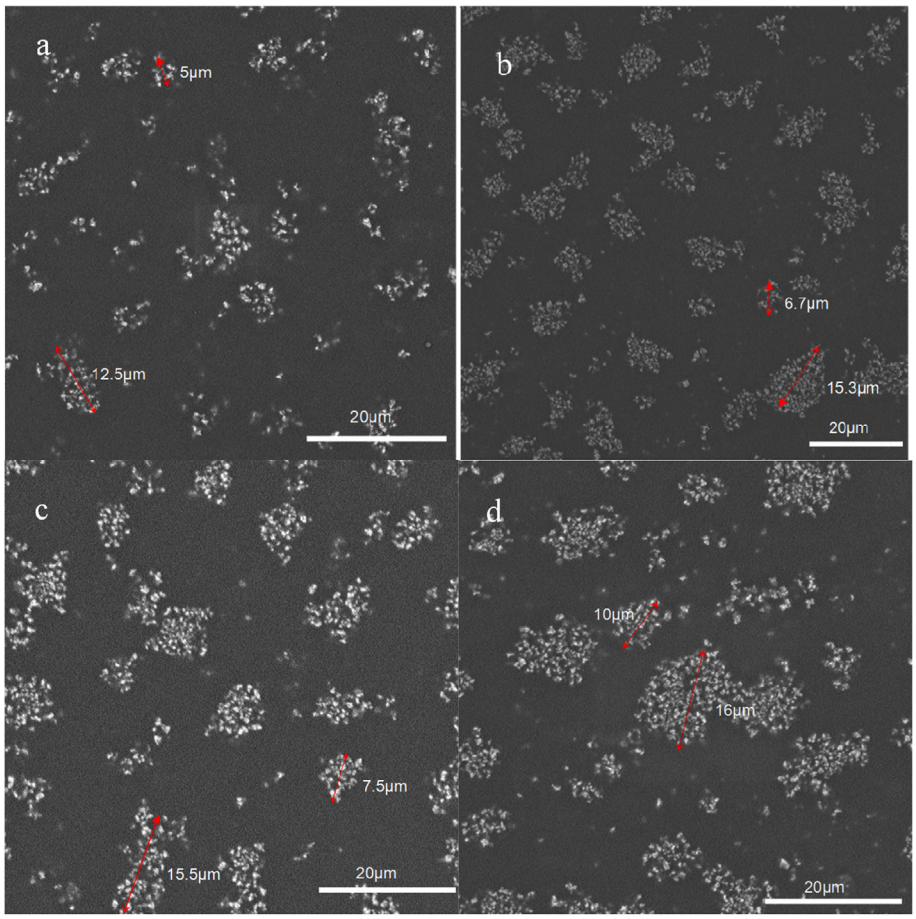

Fig. 4. SEM images of composite coating with at TiO_2 content of (a) 4 wt % (b) 6 wt % (c) 8 wt % and (d)10 wt %.

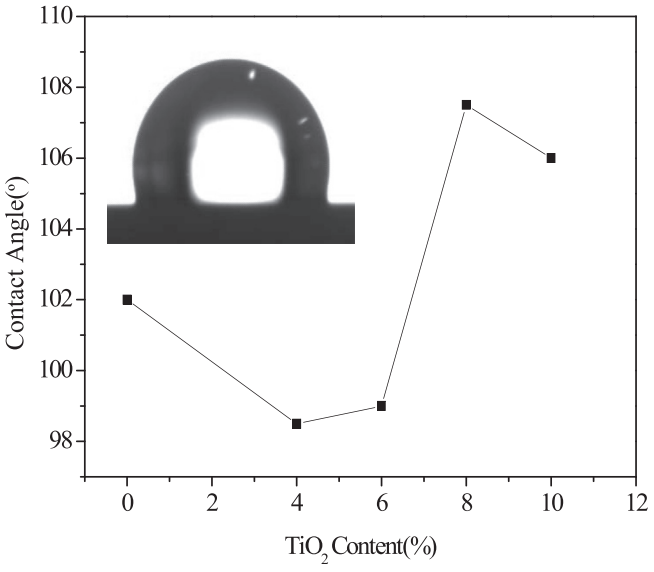

Fig. 5. Contact angle of composite coatings with different TiO_2 content.

performance. There were more micro-nano structures formed on the coating surface and the distribution of TiO_2 on the coating surface was even on the sample surface. The impedance modulus value of the coating with a TiO_2 content of 8 wt % reached up to $10^6\ \Omega\ cm^2$. Compared with bare aluminum, its impedance modulus value was two orders of magnitude higher, and its corrosion resistance had been greatly improved.

Fig. 6 (c) reveals the phase angle of bare and the composite coating with TiO_2 loading in 3.5 wt % NaCl solution. The higher the phase angle was, the stronger the hindrance to the corrosion medium [1]. As can be seen in Fig. 6 (c), bare aluminum had only one high phase angle about 80° in a very small frequency range. However, the PDMS coating had 50° phase angle in a large frequency range. When the content of TiO_2 was 6 or 8 wt %, the phase angle reached 60° in a large frequency range in Fig. 6 (c). Thus, PDMS coating with TiO_2 had a better protective effect.

The Bode and Nyquist plot of bare aluminum and coating were fitted through an equivalent circuit in Fig. 6 (a). Table 1 shows the fitting parameters about different contents of TiO_2. Among them, the physical meaning of each fitting parameter can be explained as follows. R_f representing the coating resistance was inversely proportional to the pores and defects in the coating [52]. It was extremely easy to passivate the bare aluminum, forming a layer of dense passivation coating. R_f represents passive film resistance for bare aluminum. CPE (Q) is a constant phase angle element with two parameters (Y_0, n), in which the value *n* represents the roughness of

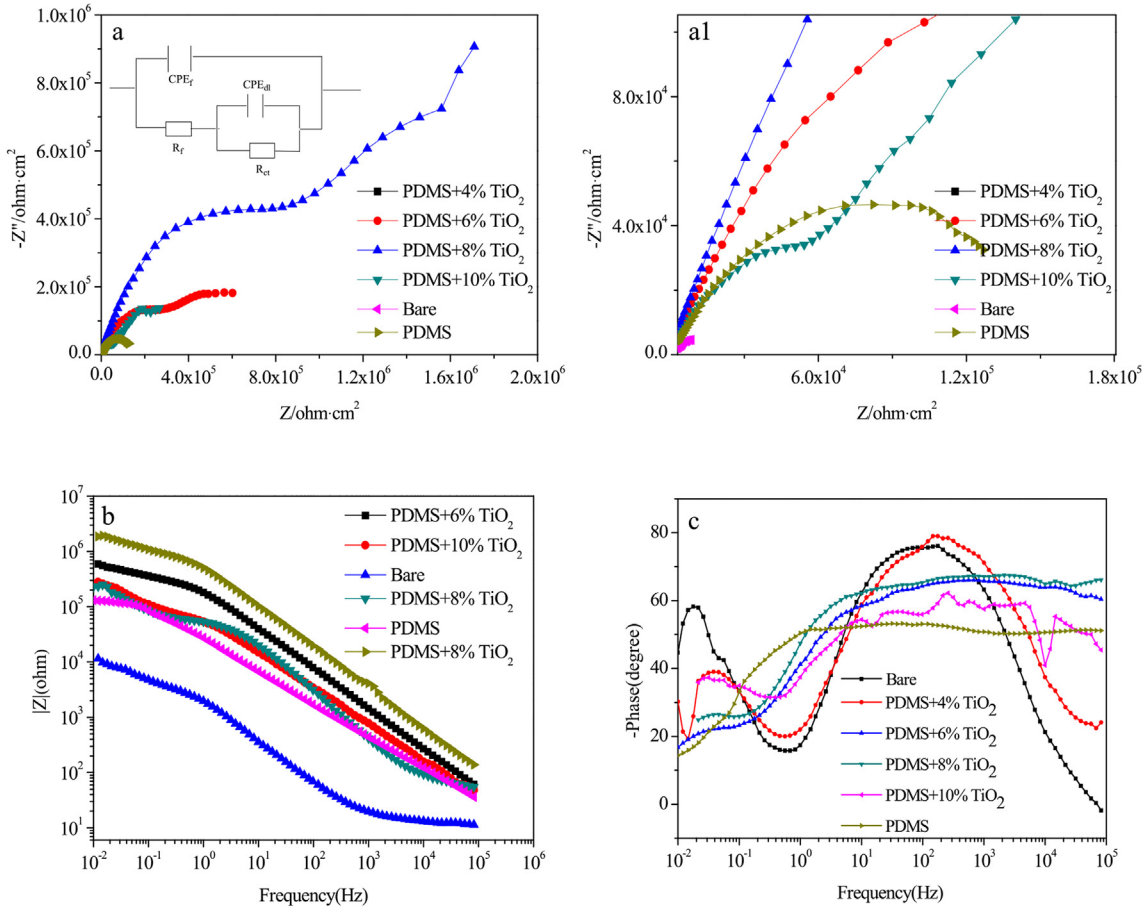

Fig. 6. Impedance diagram for PDMS/TiO_2 composite coatings (a) Nyquist diagram (a1) local enlarged drawing of Nyquist diagram (b) Bode diagram (c) Phase angle diagram.

Table 1
Equivalent circuit parameters for bare AA2024 and samples with different TiO_2 content.

Sample	R_f ($\Omega \cdot cm^2$)	CPE_{coat} (Q_{coat})		R_{ct} ($\Omega \cdot cm^2$)	CPE_{dl}(Q_{dl})	
		$Y_0(\Omega^{-1} \cdot s^n cm^{-2})$	n		Y_0 ($\Omega^{-1} \cdot s^n cm^{-2}$)	n
Bare	5317	1.05×10^{-4}	0.775	9436	7.10×10^{-4}	0.890
PDMS	872.4	6.6×10^{-6}	0.637	1.69×10^5	3.98×10^{-6}	0.622
4 wt%TiO_2	6.12×10^4	1.20×10^{-6}	0.868	2.30×10^5	3.04×10^{-5}	0.935
6 wt%TiO_2	3.94×10^5	1.09×10^{-6}	0.737	3.40×10^5	1.82×10^{-5}	0.825
8 wt%TiO_2	1.31×10^6	4.14×10^{-7}	0.744	1.16×10^6	6.28×10^{-6}	1
10 wt%TiO_2	1.15×10^5	3.8×10^{-6}	0.670	2.8×10^5	2.29×10^{-5}	0.939

the surface. Y_0 is the magnitude of the CPE [50]. Different values represent different meanings [53,54]. The R_{ct} is used to indicate the degree of ease of reaction with the metal when the corrosion medium reaches the metal surface. The larger the charge transfer impedance, the more difficult it is to react [55]. The CPE_{dl} was formed by two layers of dissimilar charges on the electrode surface. As depicted from Table 1, compared with bare aluminum, the value of R_{ct} of PDMS coating improved more than an order of magnitude, reaching $1.69 \times 10^5\ \Omega\ cm^2$. The value of Y_0 (CPE_{coat}) decreased more than two order of magnitude, reaching $6.6 \times 10^{-6}\ \Omega^{-1} \cdot s^n cm^{-2}$. After the addition of TiO_2, compared with PDMS, R_f and R_{ct} values had been greatly improved. When the content of TiO_2 was 8 wt%, R_f and R_{ct} value reached $1.31 \times 10^6\ \Omega\ cm^2$ and $1.16 \times 10^6\ \Omega\ cm^2$. Y_0 (CPE_{coat}) and Y_0 (CPE_{dl}) reached 4.14×10^{-7} and $6.28 \times 10^{-6}\ \Omega^{-1} \cdot s^n cm^{-2}$, which showed the best corrosion resistance.

3.4.2. Tafel polarization

Fig. 7 shows the Tafel curves of different samples in 3.5 wt % NaCl solution. The parameter values by Tafel extrapolation method are listed in Table 2. Parameter η was the protection efficiency and was obtained by equation [1].

$$\eta\% = \frac{I^0_{corr} - I^1_{corrt}}{I^0_{corr}} \times 100\%$$

where I^0_{corr} and I^1_{corr} were the I_{corr} of bare aluminum and different samples. As shown in Fig. 7 and Table 2, compared with bare

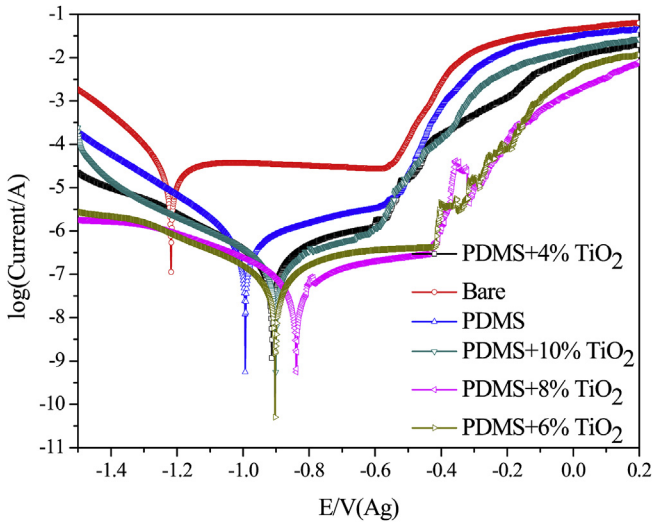

Fig. 7. Tafel polarization curves of samples with different TiO_2 content.

aluminum (-1.175 v), the E_{corr} of PDMS obviously moved 0.17 V toward positive corrosion potential. The I_{corr} of the coating was two orders of magnitude smaller than that of bare aluminum (2.714×10^{-5} A cm^{-2}), reaching 4.920×10^{-7} A cm^{-2} and η arrived 98.18%. Compared with PDMS, with increasing the TiO_2 content, the E_{corr} was more and more positive and the I_{corr} was getting smaller and smaller. When the TiO_2 content was 8 wt %, E_{corr} was the most positive. Compared with PDMS, its E_{corr} moved 0.15 V toward positive corrosion potential and the E_{corr} was the smallest, reaching 5.280×10^{-8} A cm^{-2} and η arrived 99.80%. The results showed that PDMS/TiO_2 coatings improved the anticorrosion performance.

Table 2
Tafel polarization curve parameters for bare AA2024 and different content of TiO_2.

Sample	E_{corr} (V)	I_{corr} (A·cm^{-2})	R_p	η
Bare	−1.175	2.714×10^{-5}	1523.1	
PDMS	−0.9966	4.920×10^{-7}	82181.6	98.18%
PDMS+4 wt%TiO_2	−0.9213	1.764×10^{-7}	237348.5	99.35%
PDMS+6 wt%TiO_2	−0.9047	6.383×10^{-8}	684127.1	99.76%
PDMS+8 wt%TiO_2	−0.8409	5.280×10^{-8}	839218.9	99.80%
PDMS+10 wt%TiO_2	0.9021	1.346×10^{-7}	292550.4	99.50%

3.5. Long-term immersion test

3.5.1. EIS results

The durability of coating is an important index to evaluate the quality of coating. In order to assess the long-term protective effect of coatings, the effect of the PDMS composite coating with 8 wt % TiO_2 nanoparticles on metal protection is judged by long-term immersion. The electrolyte solutions were difficult to penetrate into organic coatings due to the addition of TiO_2 in organic coatings and the diffusion of reactive particles into the organic coating was a slow process [41].

As revealed in Fig. 8(a) (the illustration is equivalent circuit),

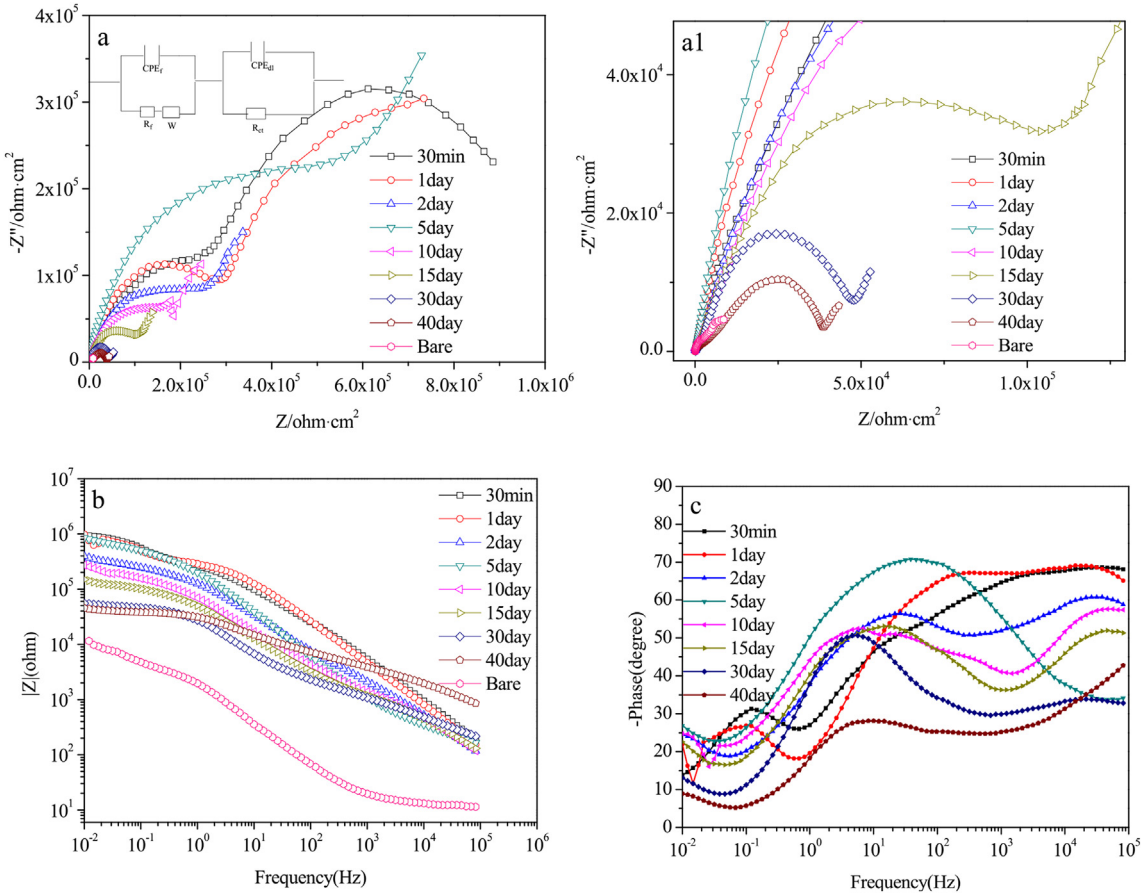

Fig. 8. Impedance diagram for composite coating with 8 wt% TiO_2 for different immersion time (a) Nyquist diagram (a1) local enlarged drawing of Nyquist diagram (b) Bode diagram (c) phase angle diagram.

when the immersion time was 30 min, the composite coating showed two large capacitive semicircles from the Nyquist diagram. Fig. 8 (a1) is local enlarged drawing of Fig. 8 (a). Higher impedance modulus value was shown in the Bode diagram in Fig. 8 (b). During the 30 min-2 d of immersion, the size with a impedance modulus value was reduced significantly from 10^6 to $10^{5.5}\,\Omega\,cm^2$ as shown in Fig. 8 (b), the equivalent circuit was shown in Fig. 6 (a). During 5-40 d of immersion, the corrosion products occurred. With the diffusion of corrosion products [56–58], a Warburg resistance element (W) can appear equivalent circuit in Fig. 8 (a). In 5-day immersion time, the impedance value was obviously improved from $10^{5.5}$–$10^6\,\Omega\,cm^2$ in Fig. 8 (b). This might be that corrosion products would obstruct the entry of electrolyte solution in the gap in diffusion process [59], so the impedance value was increased. Zhu et al. reported that the low-frequency impedance value increased after a certain immersion time. This could be interpreted as that the there are corrosion products diffused into the pores, which brought about the "pore blocking" [1]. As the immersion time went by, the electrolyte solution further penetrated into the coating, making the anticorrosion effect of the coating reduce further. The impedance modulus value became lower and lower [60]. The results indicated that the barrier of coating to corrosive medium became weaker and weaker. However, after 40 days immersion, its impedance modulus value ($10^{4.5}\,\Omega\,cm^2$) was still larger than bare sample ($10^4\,\Omega\,cm^2$) in Fig. 8 (b). Therefore, the coating still had a corrosion resistance performance. Fig. 8(c) shows that with the immersion time going by, the phase angle decreased gradually. When the immersion time was 5 days, the phase angle suddenly increased, consistent with the result of Fig. 8 (a). All these results illustrated that the composite coatings had excellent anticorrosion property.

4. Conclusion

The anticorrosion properties of PDMS coatings containing different content of TiO_2 were evaluated by Tafel and EIS in 3.5 wt % NaCl solution. The content of TiO_2 had a significant influence on the structure and properties of the composite coatings. The composite coating with 8 wt % TiO_2 possessed the best corrosion resistance. The impedance modulus value reached above $10^6\,\Omega\,cm^2$. The I_{corr} was $5.280 \times 10^{-8}\,A\,cm^{-2}$ which was three orders of magnitude Smaller than that of the bare. After adding hydrophilic TiO_2, the composite coatings remained hydrophobicity, which was excellent to improve the anticorrosion property of coating. Furthermore, after 40-day immersion, the coating still had a certain protective effect. Except anticorrosion, the polymer nanocomposites with other fillers can introduce other functions to form multifunctions in one unit such as electromagnetic interference (EMI) shielding [61,62], functional structures [63–68], sensing [70-72], and others [73].

Acknowledgements

This work was financially supported by National Nature Science Foundation of China (51572248).

References

[1] H.Z. Zhu, L.F. Yue, C. Zhuang, Fabrication and characterization of self-assembled graphene oxide/silane coatings for corrosion resistance, Surf. Coating. Technol. 304 (2016) 76–84.
[2] M.W. Khalil, Electrodeposition of Ni–GNS–TiO_2, nanocomposite coatings as anticorrosion film for mild steel in neutral environment, Surf. Coating. Technol. 275 (2015) 98–111.
[3] B.D. Mert, Corrosion protection of aluminum by electrochemically synthesized composite organic coating, Corrosion Sci. 103 (2016) 88–94.
[4] J.F. Li, S.S. Ge, J.X. Wang, et al., Water-based rust converter and its polymer composites for surface anticorrosion, Colloids Surf. A: Physicochem. Eng. Aspects 537 (2018) 334–342.
[5] Y. Feng, S. Ge, J. Li, et al., Synthesis of 3,4,5-trihydroxy-2-[(hydroxyimino) methyl] benzoic acid as a novel rust converter, Green Chem. Lett. Rev. 10 (2017) 455–461.
[6] C. Yang, H. Wei, L. Guan, et al., Polymer nanocomposites for energy storage, energy saving, and anticorrosion, J. Mater. Chem. A 3 (2015) 14929–14941.
[7] H. Wei, Y. Wang, J. Guo, et al., Advanced micro/nanocapsules for self-healing smart anticorrosion coatings, J. Mater. Chem. A 3 (2015) 469–480.
[8] Y.L. Ma, J.X. Dai, L.L. Wu, et al., Enhanced anti-ultraviolet, anti-fouling and anti-bacterial polyelectrolyte membrane of polystyrene grafted with trimethyl quaternary ammonium salt modified lignin, Polymer 114 (2017) 113–121.
[9] J. Lv, Z.Y. Liu, J. Zhang, et al., Bio-based episulfide composed of cardanol/cardol for anti-corrosion coating applications, Polymer 121 (2017) 286–296.
[10] A. Madhan Kumar, P. Sudhagar, Akira Fujishima, Zuhair M. Gasem, Hierarchical polymer nanocomposite coating material for 316L SS implants: surface and electrochemical aspects of PPy/f -CNTs coatings, Polymer 55 (2014) 5417–5424.
[11] L. Zhang, M. Qin, W. Yu, Q. Zhang, H. Xie, et al., Heterostructured TiO_2/WO_3 nanocomposites for photocatalytic degradation of toluene under visible light, J. Electrochem. Soc. 164 (2017) 1086–1090.
[12] D.D. Li, F.Y. Wang, Anticorrosion organic coating with layered double hydroxide loaded with corrosion inhibitor of tungstate, Prog. Org. Coat 71 (2011) 302–309.
[13] H. Vakili, B. Ramezanzadeh, R. Amini, The corrosion performance and adhesion properties of the epoxy coating applied on the steel substrates treated by cerium-based conversion coatings, Corrosion Sci. 94 (2015) 466–475.
[14] S. Abaci, B. Nessark, Characterization and corrosion protection properties of composite material (PANI+TiO_2) coatings on A304 stainless steel, J. Coating Technol. Res. 12 (2015) 107–120.
[15] G.S. Hikku, A. Venugopal, Corrosion resistance behavior of graphene/polyvinyl alcohol nanocomposite coating for aluminium-2219 alloy, J. Alloy. Comp. 716 (2017) 259–269.
[16] Z.A. Hamid, H.B. Hassan, Influence of electrodeposition parameters on the characteristics of NiMoP film, Surf. Coating. Technol. 212 (2012) 37–45.
[17] Z.A. Hamid, H.B. Hassan, A.M. Attyia, Influence of deposition temperature and heat treatment on the performance of electroless Ni–B films, Surf. Coating. Technol. 205 (2010) 2348–2354.
[18] C.M.P. Kumar, T.V. Venkatesha, K.G. Chandrappa, Effect of surfactants on co-deposition of B_4C nanoparticles in Zn matrix by electrodeposition and its corrosion behavior, Surf. Coating. Technol. 206 (2012) 2249–2257.
[19] A.C. Lokhande, J.S. Bagi, Studies on enhancement of surface mechanical properties of electrodeposited Ni–Co alloy coatings due to saccharin additive, Surf. Coating. Technol. 258 (2014) 225–231.
[20] B. Bakhit, A. Akbari, A comparative study of the effects of saccharin and β-SiC nano-particles on the properties of Ni and Ni–Co alloy coatings, Surf. Coating. Technol. 253 (2014) 76–82.
[21] L.J. Liu, R.F. Chen, W.K. Liu, Fabrication of superhydrophobic copper sulfide film for corrosion protection of copper, Surf. Coating. Technol. 272 (2015) 221–228.
[22] T. Ishizaki, Y. Masuda, M. Sakamoto, Corrosion resistance and durability of superhydrophobic surface formed on magnesium alloy coated with nanostructured cerium oxide film and fluoroalkylsilane molecules in corrosive NaCl aqueous solution, Langmuir 27 (2011) 4780–4788.
[23] F.H. Su, K. Yao, Facile fabrication of superhydrophobic surface with excellent mechanical abrasion and corrosion resistance on copper substrate by a novel method, ACS Appl. Mater. Interfaces 6 (2014) 8762–8770.
[24] L.B. Feng, H.X. Zhang, Z.L. Wang, Superhydrophobic aluminum alloy surface: fabrication, structure, and corrosion resistance, Colloids Surf. A: Physicochem. Eng. Aspects 441 (2014) 319–325.
[25] L.J. Liu, W.K. Liu, R.F. Chen, Hierarchical growth of Cu zigzag microstrips on Cu foil for superhydrophobicity and corrosion resistance, Chem. Eng. J. 281 (2015) 804–812.
[26] D. Lv, J. Ou, M. Xue, Stability and corrosion resistance of superhydrophobic surface on oxidized aluminum in NaCl aqueous solution, Appl. Surf. Sci. 333 (2015) 163–169.
[27] S. Shreepathi, S.M. Naik, M.R. Vattipalli, Water transportation through organic coatings: correlation between electrochemical impedance measurements, gravimetry, and water vapor permeability, J. Coating Technol. Res. 9 (2012) 411–422.
[28] M. Wang, K. Zhang, X.X. Dai, Enhanced electrical conductivity and piezoresistive sensing in multi-wall carbon nanotubes/polydimethylsiloxane nanocomposites via the construction of a self-segregated structure, Nanoscale 9 (2017) 11017–11023.
[29] K. Sun, P.T. Xie, Z.Y. Wang, Flexible polydimethylsiloxane/multi-walled carbon nanotubes membranous metacomposites with negative permittivity, Polymer 125 (2017) 50–57.
[30] K.H. Wu, C.M. Chao, C.J. Yang, Synthesis and characterization of polydimethylsiloxane-cured organically modified silicate hybrid coatings, Poly. Deg. Stab 91 (2006) 2917–2923.
[31] K. Li, X. Zeng, H. Li, Effects of calcination temperature on the microstructure and wetting behavior of superhydrophobic polydimethylsiloxane/silica coating, Colloids Surf. A: Physicochem. Eng. Aspects 445 (2014) 111–118.
[32] Y.H. Kim, M.G. Jeong, H.O. Seo, Preparation of ultrathin polydimethylsiloxane-

coating on Cu as oxidation-protection layer, Appl. Surf. Sci. 258 (2012) 7562–7566.
[33] J. Yeo, S.K. Dong, The effect of the aspect ratio on the hydrophobicity of microstructured polydimethylsiloxane (PDMS) robust surfaces, Microsystem Technol. 16 (2010) 1457–1463.
[34] X.H. Zhao, C.H. Li, H. Wang, Preparation and properties of organic-inorganic modified SiO_2 thin films, J. Cent. South Univ. B 20 (2013) 608–614.
[35] Z. Yuan, J. Bin, X. Wang, Preparation of a polydimethylsiloxane (PDMS)/$CaCO_3$, based superhydrophobic coating, Surf. Coating. Technol. 254 (2014) 97–103.
[36] G. Ruhi, H. Bhandari, S.K. Dhawan, Designing of corrosion resistant epoxy coatings embedded with polypyrrole/SiO_2 composite, Prog. Org. Coat 77 (2014) 1484–1498.
[37] R.C. Barik, J.A. Wharton, R.J.K. Wood, Corrosion, erosion and erosion–corrosion performance of plasma electrolytic oxidation (PEO) deposited Al_2O_3 coatings, Surf. Coating. Technol. 199 (2005) 158–167.
[38] A. Mostafaei, F. Nasirpouri, Epoxy/polyaniline–ZnO nanorods hybrid nanocomposite coatings: synthesis, characterization and corrosion protection performance of conducting paints, Prog. Org. Coat 77 (2014) 146–159.
[39] E. Matin, M.M. Attar, B. Ramezanzadeh, Investigation of corrosion protection properties of an epoxy nanocomposite loaded with polysiloxane surface modified nanosilica particles on the steel substrate, Prog. Org. Coat 78 (2015) 395–403.
[40] B. Ramezanzadeh, E. Ghasemi, M. Mahdavian, Covalently-grafted graphene oxide nanosheets to improve barrier and corrosion protection properties of polyurethane coatings, Carbon 93 (2015) 555–573.
[41] J. Ejenstam, A. Swerin, J. Pan, Corrosion protection by hydrophobic silica particle-polydimethylsiloxane composite coatings, Corrosion Sci. 99 (2015) 89–97.
[42] H.L. Zhao, W. Deng, Y. Li, Atomic layer deposited TiO_2, ultrathin layer on Ag_ ZnO nanorods for stable and efficient photocatalytic degradation of RhB, Adv. Comp. Hybrid Mater (2018) in press, https://doi.org/10.1007/s42114-017-0015-0.
[43] L. Zhang, W. Yu, C. Han, et al., Large scaled synthesis of heterostructured electrospun TiO_2/SnO_2 nanofibers with an enhanced photocatalytic activity, J. Electrochem. Soc. 164 (2017) 651–656.
[44] Q.Y. Wang, P. Yu, L. Bai, et al., Self-assembled nano-leaf/vein bionic structure of TiO_2/MoS_2 composites for photoelectric sensors, Nanoscale 9 (2017) 18194–18201.
[45] B. Song, T.T. Wang, H.G. Sun, et al., Two-step hydrothermally synthesized carbon nanodots/WO_3 photocatalysts with enhanced photocatalytic performance, Dalton Trans. 46 (2017) 15769–15777.
[46] Y. Qing, C. Yang, Y. Sun, Facile fabrication of superhydrophobic surfaces with corrosion resistance by nanocomposite coating of TiO_2 and polydimethylsiloxane, Colloids Surf. A: Physicochem. Eng. Aspects 484 (2015) 471–477.
[47] S. Zhai, B. Zhai, Q. An, Effect of preparation conditions on structural properties of PMHS-TEOS hybrid materials, J. Sol. Gel Sci. Technol. 59 (2011) 480–487.
[48] L. Téllez, J. Rubio, F. Rubio, FTR study of the hydrolysis and polymerization of tetraethyl orthosilicate and polydimethyl siloxane in the presence of tetrabutyl orthotitanate, Spectrosc. Lett. 37 (2004) 11–31.
[49] V.M. Gun'Ko, V.V. Turov, Characterization of fumed alumina/silica/titania in the gas phase and in aqueous suspension, J. Colloid Interface Sci. 220 (1999) 302–323.
[50] L.J. Li, J.X. He, J.L. Lei, A sol–bath–gel approach to prepare hybrid coating for corrosion protection of aluminum alloy, Surf. Coating. Technol. 279 (2015) 72–78.
[51] J.B. Bajat, I. Milošev, Ž. Jovanović, Corrosion protection of aluminium pretreated by vinyltriethoxysilane in sodium chloride solution, Corrosion Sci. 52 (2010) 1060–1069.
[52] M. Yan, C.A. Vetter, V.J. Gelling, Corrosion inhibition performance of polypyrrole Al flake composite coatings for Al alloys, Corrosion Sci. 70 (2013) 37–45.
[53] VadimF. Lvovich, Impedance Spectroscopy: Applications to Electrochemical and Dielectric Phenomena, Wiley, 2012, pp. 97–111.
[54] G.Q. Xia, X.H. Jiang, L.M. Zhou, Synergic effect of methyl acrylate and N-cetylpyridinium bromide in N-cetyl-3-(2-methoxycarbonylvinyl)pyridinium bromide molecule for X70 steel protection, Corrosion Sci. 94 (2015) 224–236.
[55] X. Yuan, Z.F. Yue, X. Chen, The protective and adhesion properties of silicone-epoxy hybrid coatings on 2024 Al-alloy with a silane film as pretreatment, Corrosion Sci. 104 (2016) 84–97.
[56] P. Wang, D. Zhang, R. Qiu, Super-hydrophobic film prepared on zinc as corrosion barrier, Corrosion Sci. 53 (2011) 2080–2086.
[57] L.J. Liu, W.K. Liu, R.F. Chen, Hierarchical growth of Cu zigzag microstrips on Cu foil for superhydrophobicity and corrosion resistance, Chem. Eng. J. 281 (2015) 804–812.
[58] S. Yuan, S.O. Pehkonen, B. Liang, Superhydrophobic fluoropolymer-modified copper surface via surface graft polymerization for corrosion protection, Corrosion Sci. 53 (2011) 2738–2747.
[59] P.S. Correa, C.F. Malfatti, D.S. Azambuja, Corrosion behavior study of AZ91 magnesium alloy coated with methyltriethoxysilane doped with cerium ions, Pro. Org. Coat 72 (2011) 739–747.
[60] G.L. Song, A. Atrens, Corrosion mechanisms of magnesium alloys, Adv. Eng. Mater. 1 (2010) 11–33.
[61] K. Zhang, G. Li, L. Feng, et al., Ultralow percolation threshold and enhanced electromagnetic interference shielding in poly(L-lactide)/multi-walled carbon nanotubes nanocomposites with electrically conductive segregated networks, J. Mater. Chem. C 5 (2017) 9359–9369.
[62] N. Wu, J. Qiao, J. Liu, et al., Strengthened electromagnetic absorption performance derived from synergistic effect of carbon nanotube hybrid with Co@C beads, Adv. Comp. Hybrid Mater. (2018), https://doi.org/10.1007/s42114-017-0008-z in press.
[63] J. Gu, W. Dong, Y. Tang, et al., Ultra-low dielectric fluoride-containing cyanate ester resins combined with improved mechanical properties and high thermal & dimension stabilities, J. Mater. Chem. C 5 (2017) 6929–6936.
[64] X. Wang, X. Liu, H. Yuan, et al., Non-covalently functionalized graphene strengthened poly(vinyl alcohol), Mater. Des. 139 (2018) 372–379.
[65] Z. Hu, C. Wang, F. Zhao, et al., Fabrication of a graphene/C60 nanohybrid via gamma-cyclodextrin host-guest chemistry for photodynamic and photothermal therapy, Nanoscale 9 (2017) 8825–8833.
[66] C. Wang, M. Zhao, J. Li, et al., Silver nanoparticles/graphene oxide decorated carbon fiber synergistic reinforcement in epoxy-based composites, Polymer 131 (2017) 263–271.
[67] Z. Hu, Q. Shao, M. Moloney, et al., Nondestructive functionalization of graphene by surface-initiated atom transfer radical polymerization: an ideal nanofiller for poly(p-phenylene benzobisoxazole) fibers, Macromolecules 50 (2017) 1422–1429.
[68] W. Zhao, J. Kong, H. Liu, et al., Ultra-high thermal conductivity and rapid heat response in self-aligned graphene/poly(benzobisoxazole) nanocomposites, Nanoscale 8 (2016) 19983–19994.
[69] Z. Hu, D. Zhang, L. Yu, Y. Huang, Light-triggered C60 release from a graphene/cyclodextrin nanoplatform for the protection of cytotoxicity induced by nitric oxide, J. Mater. Chem. B 6 (2018) 518–526.
[70] Y. Li, B. Zhou, G. Zheng, et al., Continuously prepared highly conductive and stretchable SWNTs/MWNTs synergistically composited electrospun thermoplastic polyurethane yarns for wearable sensing, J. Mater. Chem. C (2017), https://doi.org/10.1039/C7TC04959E in press.
[71] H. Liu, W. Huang, X. Yang, et al., Organic vapor sensing behaviors of conductive thermoplastic polyurethane-graphene nanocomposites, J. Mater. Chem. C 4 (2016) 4459–4469.
[72] J. Zhao, L. Wu, C. Zhan, et al., Overview of polymer nanocomposites: computer simulation understanding of physical properties, Polymer 133 (2017) 272–287.
[73] H. Gu, C. Liu, J. Zhu, et al., Introducing advanced composites and hybrid materials, Adv. Comp, Hybrid Mater (2018) in press, https://doi.org/10.1007/s42114-017-0017-y.